A new automated system for combined luminescence and exo-electron measurements

Autzen, Martin; Poolton, Nigel Robert James; Murray, A. S.; Kook, Myung Ho; Buylaert, Jan-Pieter

Published in:
Nuclear Inst. and Methods in Physics Research, B

Link to article, DOI:
10.1016/j.nimb.2019.01.030

Publication date:
2019

Document Version
Publisher's PDF, also known as Version of record

Nuclear Inst. and Methods in Physics Research B 443 (2019) 90–99

Contents lists available at ScienceDirect

Nuclear Inst. and Methods in Physics Research B

journal homepage: www.elsevier.com/locate/nimb

A new automated system for combined luminescence and exo-electron measurements

M. Autzen[a,*], N.R.J. Poolton[a], A.S. Murray[b], M. Kook[a], J.-P Buylaert[a,b]

[a] Center for Nuclear Technologies, Technical University of Denmark, DTU Risø Campus, DK-4000 Roskilde, Denmark
[b] Nordic Laboratory for Luminescence Dating, Department of Geoscience, Aarhus University, Risø Campus, DK-4000 Roskilde, Denmark

ARTICLE INFO

Keywords:
TL
OSL
TSE
OSE
Exo-electrons
HV-modulation

ABSTRACT

The measurement of OSL/TL relies on the initial trapping and subsequent release and recombination of charge in a suitable crystal structure. These measurements allow us to estimate the dose which the crystal has been subjected to and its age. During such processes, however, electrons can be emitted from the sample surface; the ability to measure such exo-electrons can provide information regarding the trapping process, as well as an alternative method of measuring trapped charge. Ideally, TL/OSL can be measured alongside exo-electrons.

We will present a new design for an exo-electron detector compatible with the classic Risø reader stimulation head featuring multiple anode configurations and the option for high-voltage modulation to reduce the UV component during TL/OSL measurements.

1. Introduction

Here we describe a new instrument for the simultaneous measurement of electrons and photons emitted from minerals during optical and/or thermal stimulation. In trapped charge dosimetry, as energy is absorbed from ionising radiation, charge is trapped at defects in the crystal lattice of wide band gap insulators. This trapped charge can be released by stimulation with heat or light leading to the emission of photons, called thermoluminescence (TL) and optically stimulated luminescence (OSL), respectively. It can also be probed directly in the trap using Electron Paramagnetic Resonance (EPR/ESR) (e.g. [9]. These phenomena are known for both natural (e.g. quartz and feldspars, [8,17,18]) and artificial materials (BeO, Al_2O_3, etc. [9,11,10]. Luminescence relies on the recombination of an electron with a hole trapped at a separate site and is thus only an indirect measure of the trapped charge. On the other hand, exo-electron emission [13], where stimulated electrons escape the crystal surface, does not depend on recombination, and so provides a direct approach to the measurement of stimulated electrons. Thus, a comparison of changes in exo-electron and luminescence response to dose should provide valuable information about luminescence efficiency, and recombination pathways and probabilities.

Exo-electron emission describes the release of electrons from a surface that has been exposed to ionising radiation This can be either a one-step or two-step process, most likely either photon or phonon stimulation, or photon-phonon (thermally assisted photo eviction) or phonon-phonon process [13]. Other processes such as photon-photon stimulation are possible but unlikely [13]. In the one-step model, an electron is stimulated from a trap by heat or light, and enters the conduction band. If it has sufficient remaining energy to overcome the electron affinity it can escape the surface (Fig. 1). In the two-step model the electron is only given sufficient energy to enter the conduction band. There it acquires sufficient additional energy to overcome the electron affinity (Fig. 1).

Exo-electrons arising from thermal stimulation (here for consistency TSE rather than more commonly used TSEE) were first observed by Tanaka in the period 1935–1940 [13]; he c surfaces of metal oxides which had previously been exposed to ionising radiation. A comprehensive list of materials emitting TSE can be found in Becker [24].

When exo-electrons leave the crystal surface they will normally react rapidly with any electrophilic species such as water vapour. But if this reaction is minimised, these exo-electrons become available for measurement, for instance using an electron multiplier or a gas counter [19]. TSE studies on natural materials have been carried out on ceramics [22] and fired quartz [23] using gas counters. Ref. [6] studied powdered human enamel and enameloid from a Great White shark without any chemical or thermal treatment. In [7] he chemically treated sediments with 0.1 M hydrochloric acid and 30% hydrogen peroxide to remove carbonate and organic matter before TSE measurements. [1–3] and Tsukamoto et al. [16] also used a gas counter and

* Corresponding author.
E-mail address: maaut@dtu.dk (M. Autzen).

https://doi.org/10.1016/j.nimb.2019.01.030
Received 20 November 2018; Accepted 21 January 2019
Available online 08 February 2019

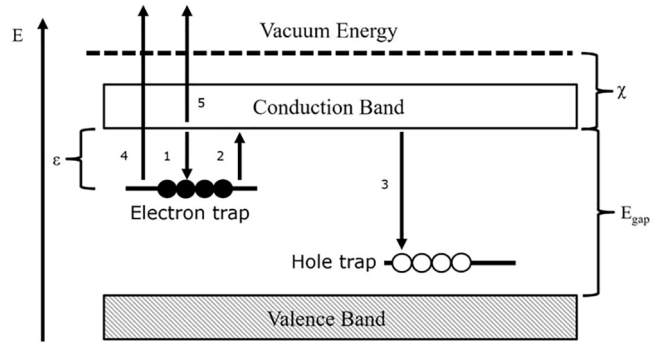

Fig. 1. Band diagram showing the pathways of exo-electrons and luminescence emission in wide band-gap materials. Trapping of electrons in traps occurs via (1). These electrons can then be stimulated into the conduction band (2) using heat or light. From the conduction band they can recombine with trapped holes and emit luminescence (3). Exo-electron emission (4, one-step process) and (5, two-step process) does not rely on recombination but (4) is only possible if the absorbed stimulation energy is greater than the sum of the trap depth (ε) and electron affinity (χ).

chemically cleaned quartz and feldspar extracted from sediments for their measurements. Ankjærgaard et al. [1] were the first to measure Optically Stimulated Exo-Electrons (OSE). Their exo-electron detector was used with an automated Risø TL/OSL reader; this combination allowed automatic irradiation, thermal pretreatment and repeated simultaneous measurement of TL/OSL with TSE/OSE. However the luminescence signals were contaminated by a strong UV gas-fluorescence signal resulting from the ionization of the counting gas (argon) during electron acceleration; de-excitation produces gas fluorescence (see Fig. 4 in [1]. As a result, luminescence measurements had to be carried out separately from exo-electron measurements to avoid the contaminating UV signal. This had serious implications for the measurement of naturally irradiated materials (such as are used in luminescence dating): when measuring aliquots of such material, it was not possible to obtain a TL/OSL signal and a TSE/OSE signal from the same aliquot during the same measurement cycle. Here we present a new Risø Exo-Electron System (REES), based on a flow-through gas detector operated in the Geiger-Müller (GM) region. The system has a modular design that allows the user to easily change the distance from the gas-detector anode to sample or switch to a different anode configuration, with the intention of maximising detection efficiency for both exo-electrons and luminescence. It also employs high-voltage switching to separate the OSL signal from UV fluorescence, and it can be used with both broad-field and focussed laser beam stimulation.

2. Design and construction

2.1. Design specifications

REES was designed with several goals in mind: (i) it should be compatible with the existing automated Risø TL/OSL reader able to accommodate up to 48 individual subsamples (aliquots) on a turntable, (ii) it should be capable of measuring TL/OSL and TSE/OSE simultaneously from the same aliquot – this suggests that the UV fluorescence from the Ar filler gas should be minimised during luminescence measurement, (iii) since the UV fluorescence is caused by the acceleration of exo-electrons, the detector should be able to measure the UV fluorescence as a surrogate for exo-electrons, and finally (iv) the detector must be sufficiently sensitive to detect exo-electrons resulting from typical burial doses (e.g. 10 Gy) from natural minerals including quartz and feldspar. Items (ii) and (iii) in the above are, of course, to some degree incompatible with each other.

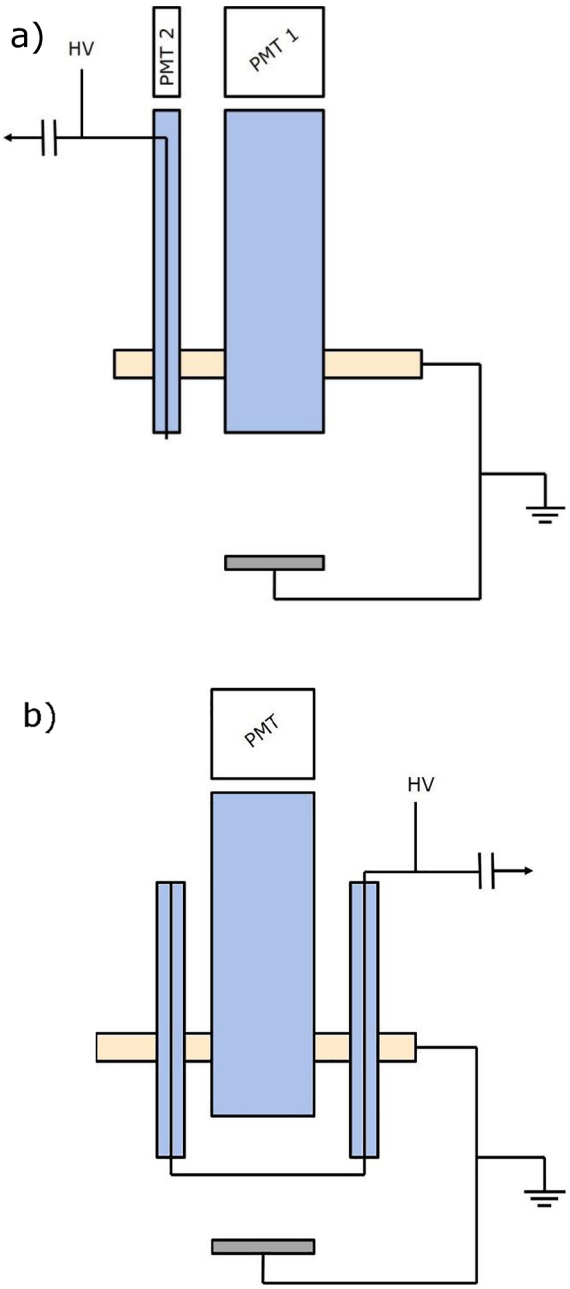

Fig. 2. Schematic of REES. a) point anode configuration with separate PMT (PMT2) to detect gas fluorescence. b) linear and circular anode configuration. The central light guide located under the PMT collects the TL/OSL. At the bottom of the view is the sample disc which sits on a heater plate connected to earth. Quartz components are shown in light blue, cathode grounding plate is shown in light yellow and the sample in dark gray.

2.2. Design of REES

REES is based around a GM detector mounted inside the Risø TL/OSL reader stimulation head for combined luminescence and exo-electron measurements. In order to minimise the contamination of the luminescence signal by gas fluorescence, three different anode configurations were chosen to physically separate the volume in which the UV is generated, from the optical path of the luminescence. As well as this spatial separation, the HV supply to the anode can be pulsed during stimulation (0–3 kHz, user defined mark/space ratio, rise/fall time of applied voltage approx. 3 μs). This is intended to allow the

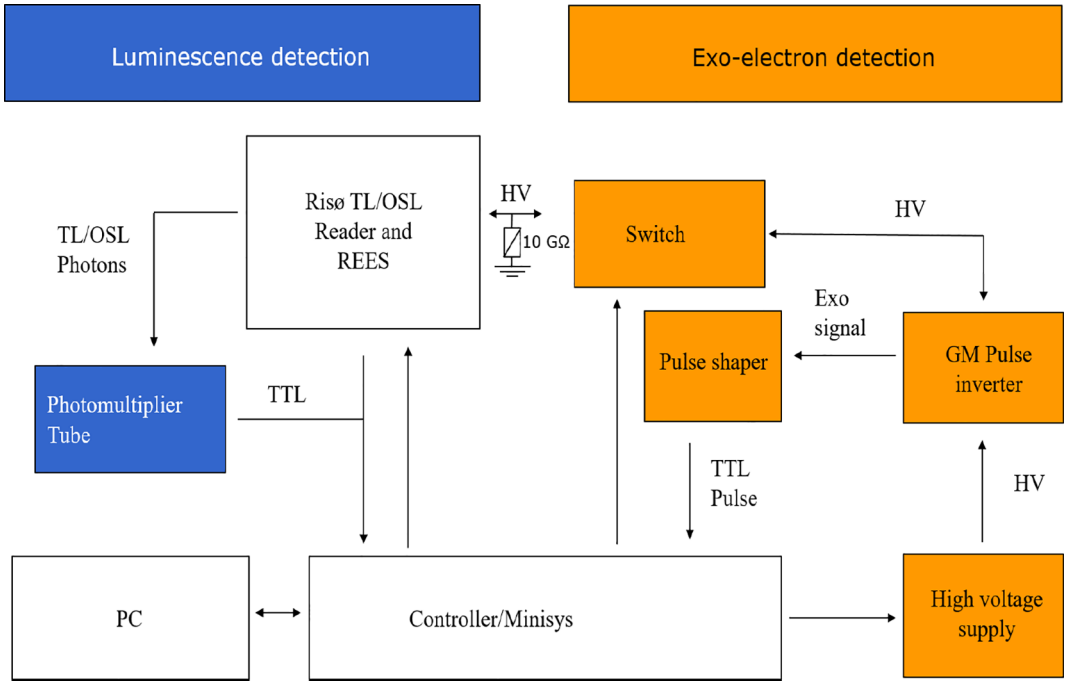

Fig. 3. Schematic of REES integration with the standard Risø TL/OSL measurement platform. It is worth noting that the 10 GΩ resistor allows the exo-electron signal to decay much faster than the switching time when using pulsed HV.

measurement of TL/OSL in the absence of electron multiplication (and so UV fluorescence) during the off-period. By interpolation, the uncontaminated luminescence signal can be subtracted from the combined UV and luminescence measured during the on-period, to give a pure gas fluorescence signal – providing a separate measurement of TSE/OSE. The point anode design (see later sections) also features a second PMT, which directly measures the UV generation around the anode (Fig. 2a).

Although REES is modular and allows for different anode configurations there are several parts in common. The detection volume is contained within a quartz tube glued to the bottom flange in the stimulation head of a Risø TL/OSL reader; the entire reader volume, including detector, can be evacuated down to 0.1 mB prior to flushing with counting gas. The detection unit itself can be removed from the quartz tube to change the anode configuration or replace the 100 µm diameter anode wire.

The detection unit is built around a central, solid quartz rod, which also functions as a central light guide for collecting luminescence from the sample (Fig. 2). The different anode configurations are supported by separate quartz pipes, to reduce the risk of arcing to the earthed surfaces, and are supported by a secondary platform held in place on the central light guide. Vertical adjustment of the quartz pipes containing the anode wire allows easy manipulation of the sample/anode distance. The sample is located at the bottom of the detection volume; this is lifted into position by a movable heating plate (part of the reader platform). A MACOR ring (not shown) is placed around the sample to reduce the risk of arcing from the anode to the corners of the bottom flange.

A schematic diagram illustrating the integration of REES with the Risø TL/OSL reader is shown in Fig. 3. Exo-electrons are collected at the anode and the resulting voltage pulse is passed through a Spectrum Techniques Inc. GM Tube Pulse Inverter (model GPI) and transformed into TTL pulses before passing to the control computer (Minisys, see Fig. 3). The measurement chamber is first evacuated and thereafter flushed with a 1% Ar-isobutane gas mixture at a flow rate of 0–0.5 l/min, while maintaining a set pressure (typically 1000 mB) using an Alicat PC15PSIA-D/5P flow-meter. The standard programmable control software (Sequence Editor) running on the host PC has been modified to provide automatic control of HV switching and synchronised counting of pulses from the anode and from the luminescence detector.

2.3. Modelling

Electric field modelling of each anode configuration was done using COMSOL Multiphysics©[1] to predict the functioning of the various configurations. This allows us to confirm that the electric field lines (presumably tracked by the exo-electrons and cascade electrons) from the sample will reach the anode. Fig. 4 shows the modelling results and a bottom view image of the different anode configurations.

2.3.1. Ring anode

The ring anode configuration is one option for spatially separating TL/OSL and TSE/OSE by moving the anode away from the central light guide (Fig. 4a–c). It is possible to change the radius (typically ~7 mm) of the ring. Here we can see that the electric field lines do not go through the central light guide, although there is some electric potential, but primarily terminate at the anode.

2.3.2. Point anode

The point anode configuration is another option to spatially separate TSE/OSE from the TL/OSL but it also provides a secondary method for detection of TSE/OSE using gas fluorescence (Fig. 4d–f). Most of the gas fluorescence will be generated in the region of the point anode as the argon gas is ionized and the resulting UV photons are guided up the quartz pipe and reflected into a separate, secondary PMT. This may be a more sensitive method for detecting TSE/OSE than direct electric measurements. The radial location of the anode is fixed due to location of the quartz pipe, but it is possible to adjust the length of wire exposed to the counting volume. Using a point anode, flush with the light guide, all the field lines from the sample terminate at the anode tip; although

[1] COMSOL Multiphysics® v. 5.2. www.comsol.com. COMSOL AB, Stockholm, Sweden.

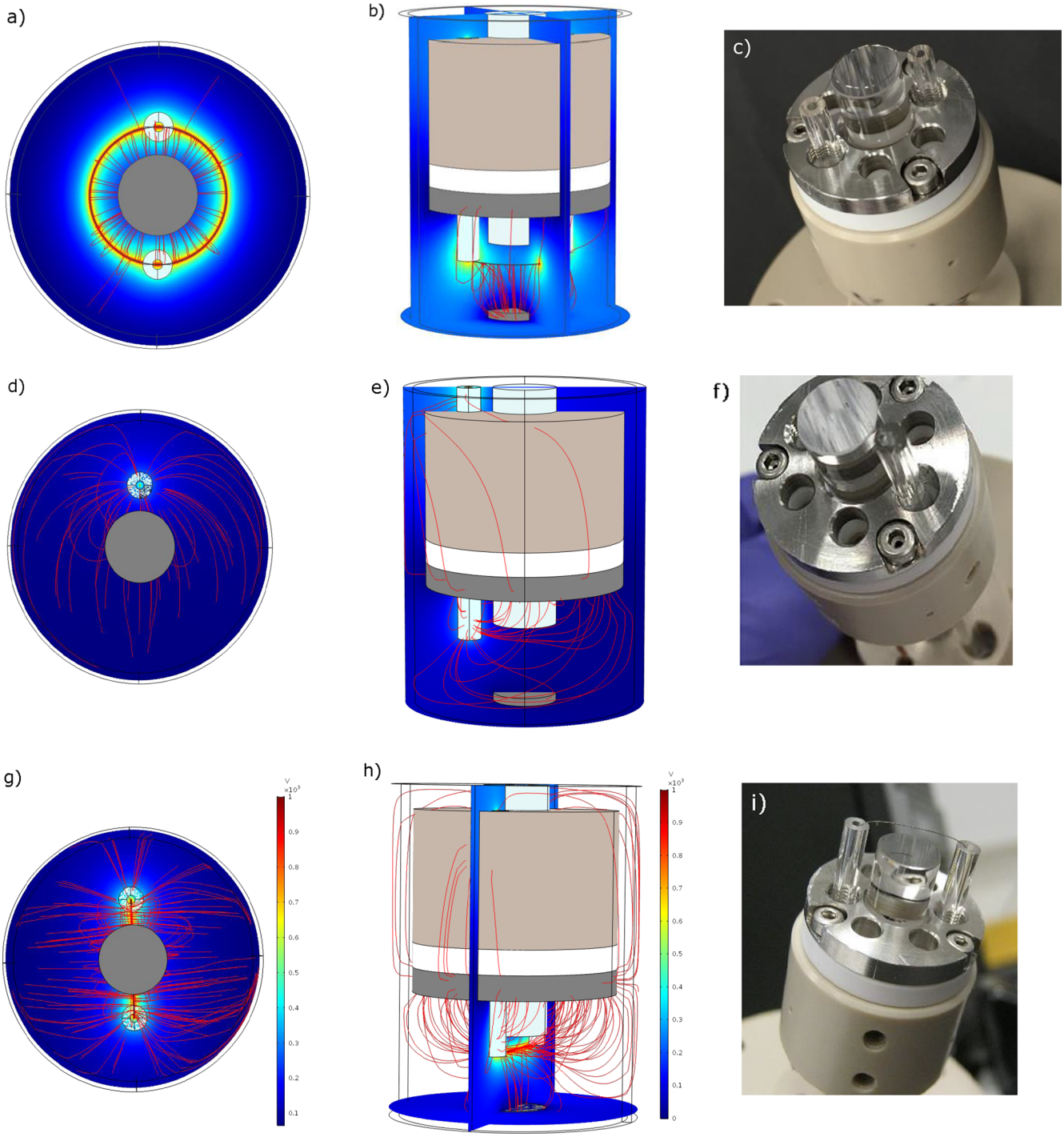

Fig. 4. Electric field modelling and photographs of ring anode (a-c), point anode (d–f) and linear anode (g–i) configurations. a, d, and g show a view of the detector from below, with the sample disc in the centre. b, e, and h show 3D modelling of the electric field lines. c, f, and i are photographs of the three anode configurations.

the quartz tube intersects a few lines, only a small fraction of accelerating electrons in the avalanche will follow these lines and so will not be fully imaged on the anode. Since the detector operates in GM mode (i.e. charge saturation) moderate fluctuations in the number of accelerated electrons are very unlikely to affect the presence or absence of an anode pulse. Thus there is unlikely to be a significant advantage in exposing more wire, but there will be an increased risk of arcing to the ground plate.

2.3.3. *Linear anode*

The linear anode design is shown in Fig. 4g–i. This anode configuration is similar to that used by [1–3] and Tsukamoto et al. [16], except that it does not have a grid cathode on the opposite side of the anode from the sample. This configuration does not attempt to spatially separate TL/OSL from TSE/OSE as the other designs do, but it may provide greater detection efficiency due to the proximity of the anode to ground – the linear anode design has no horizontal offset and is thus

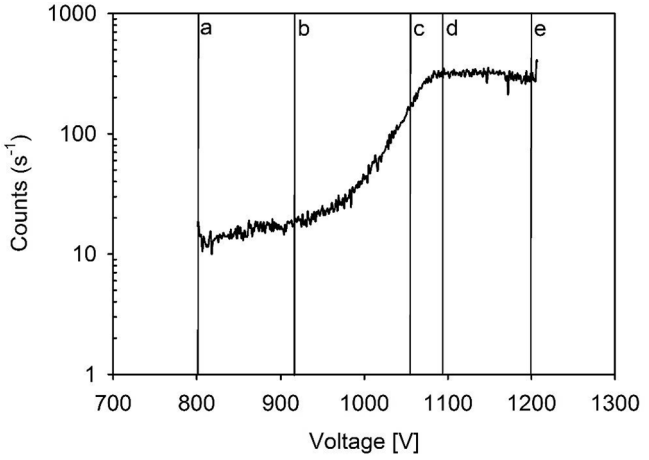

Fig. 5. Example of the variation in counting efficiency with anode voltage produced using REES and a ^{63}Ni ($\bar{E}$ = 17 keV) source deposited on stainless steel and held at 50 °C. The curve can be divided into several regions: a) ion-chamber, b) proportional, c) semi-proportional, d) Geiger plateau, and e) electrical breakdown.

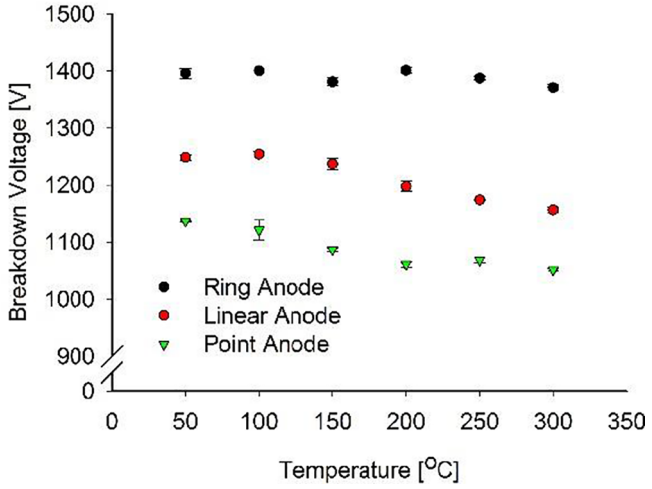

Fig. 6. Dependence of breakdown voltage on sample temperature The error bars are the standard error for three runs.

closer to grounded surfaces compared to the point or ring anode at the same vertical distance. Thus for the linear anode, it is more likely that exo-electrons emitted obliquely will be accelerated sufficiently to cause an avalanche before becoming attached to an electrophilic impurity in the gas; on the other hand, it is possible that this proximity will also increase the chance of arcing.

It can be seen from Fig. 4h that all the field lines originating from the sample terminate at the anode wire and that due to the position of the wire there is a very low probability of field lines passing through the central light guide. The risk of arcing appears to be greatest where the anode makes a sharp turn when coming out of the quartz pipes as this increases the local field strength.

3. Characterisation of the instrument

Here we document the detector characteristics (efficiency curve, arcing voltage, pressure dependence, HV switching, etc.) of the REES gas detector based system.

A gas detector can operate in several different regions (defined as ion-chamber, proportional, semi-proportional, Geiger plateau and breakdown), each with certain advantages and disadvantages. These regions are usually identified by the relationship of pulse height with applied voltage, but the efficiency relationship follows a similar shape, and so the traditional region names remain useful. In Fig. 5 these regions are illustrated using an efficiency curve measured using REES with a ^{63}Ni source ($\bar{E} = 17keV$, $E_{max} = 66keV$, average Continuous Slowing Down Approximation (CSDA) range in argon ~0.5 cm); each region has a different relationship between efficiency and voltage. In the ion-chamber region, the number of ionization events in the gas is proportional to the initial electron energy, and so the total charge mirrored at the anode in each pulse is proportional to the energy of the individual electrons emitted by the source. Unfortunately, the efficiency in this region is very low, because electrons are not accelerated sufficiently to induce gas multiplication and many are lost to recombination. In the proportional counting region (b), multiplication does take place, and so progressively fewer electrons are lost to recombination as the voltage increases; this gives rise to a steady increase in efficiency with voltage. In the semi-proportional region (c), between the proportional and Geiger region, almost all electrons give rise to a signal, but the amplitude of each pulse can vary, and so some may still fall below the counting threshold. Finally, in the Geiger region (d), an electron multiplication avalanche saturates the gas surrounding the length of the anode. As a result, all pulses have the same amplitude, and this is independent of the applied voltage; since essentially all emitted electrons give rise to a pulse, the count rate is cregion for our experiments because it is the most sensitive to the very low energies expected from exo-electrons. At increasingly higher voltages, electrical breakdown begins (e).

3.1. Breakdown using thermo-ionic emission

Breakdown, or arcing, occurs when the voltage reaches the threshold for spontaneous breakdown in the gas. This voltage is dependent on pressure, temperature and the distance to the grounded sample plate. Since we keep the pressure, and the sample to anode distance fixed, we need only investigate the dependence on temperature, using empty, undosed stainless steel cups as the cathode. These are the same cups as are used for routine luminescence and exo-electron measurements and should provide a good indication of the manner in which the breakdown voltage can be expected to occur at different temperatures. The addition of exo-electrons from materials (usually grains) held in the steel cups may slightly lower this arcing voltage.

The temperature dependence was investigated by bringing the cup to a given temperature between 50 °C and 300 °C and then increasing the voltage at a rate of 1 V/s until arcing is achieved (the chamber was kept at constant pressure of 1000 mbar). This experiment was repeated for the three different anode configurations and the results are shown in Fig. 6.

The linear and point anodes show a drop in breakdown voltage as the temperature is increased while the ring anode remains stable around 1400 V. This means that, when using the ring anode, it would be possible to keep a significantly higher fixed voltage across the temperature ranges normally used in OSL dating applications (at least from the point of view of breakdown) than for the other two anode configurations.

3.2. Temperature dependence of efficiency

Luminescence production from quartz and other natural materials is known to be affected by a variety of parameters, including thermal pretreatment and measurement temperature [14,5] p. 74; [20,21]). As

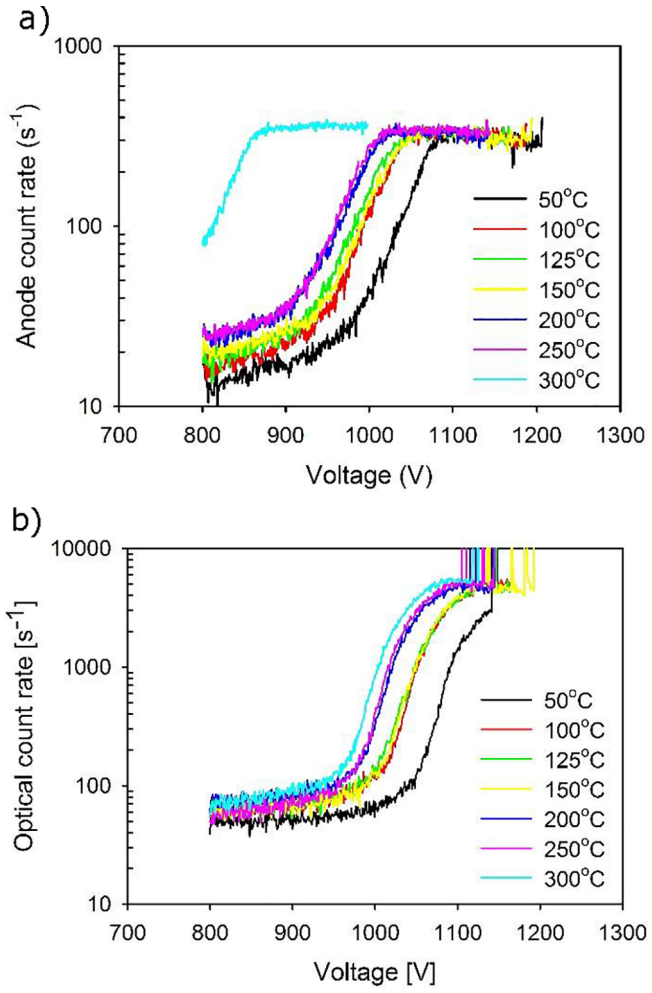

Fig. 7. Efficiency as a function of source temperature using a ^{63}Ni source mounted on a stainless steel cup and the linear anode configuration. As the temperature is increased, both the proportional region and breakdown starts at a progressively lower anode voltage. a) Anode count rate as a function of voltage. The count rates are essentially independent of temperature in the plateau region. b) The UV intensity corresponding to the anode count rate in a). The electron:UV ratio on the plateau is independent of temperature (note that the 50 °C UV data do not reach the plateau before breakdown.

a result, exo-electron measurements may also be affected by sensitivity changes, since luminescence production and exo-electron emission are competing processes (Fig. 1. In addition, thermal assistance is likely to allow electrons from deeper below the crystal surface to escape, increasing the crystal volume available as an exo-electron source; thermal assistance can also help electrons to escape the surface even if the stimulation light does not deliver sufficient energy [13]. But to investigate these dependencies, it is clearly important that the detector efficiency is temperature independent, or at least that any dependence is well known. To investigate such efficiency dependence, the ^{63}Ni source discussed above was used as a temperature-independent source of electrons. Using this source, we have constructed efficiency curves as a function of temperature for each different anode configuration.

It can be seen from Fig. 7a and b that as the temperature increases we achieve proportional counting at a lower voltage. Assuming that the thermionic background emission of electrons from stainless steel does not change significantly in this low temperature region (50–290 °C), these data suggest that the gain of the gas increases with increasing temperature, presumably because the argon becomes easier to ionize. Fig. 6 shows that the arcing voltage also decreases with increasing temperature for an empty, undosed stainless steel cup; the decrease is most pronounced for the linear and point anode configurations. The anode and UV signals appear to follow separate efficiency curves. At 1100 V, the anode signal at 50 °C is firmly on the plateau while the UV curve is still climbing, the reason for this is unknown.

The detection efficiencies for the different anodes are presented in Table 1. The measurements were performed by keeping the ^{63}Ni source at 125 °C and increasing the voltage by 1 V s^{-1} and using the count rates in the GM region.

Table 1 shows that the ring anode is 33% less efficient than the linear anode, and the point anode (and the UV signal recorded by PMT2) 79% less efficient. It is clear that the linear anode gives the highest count rate and would thus also appear to be the most sensitive. However, the ring anode is much more efficient in reducing the UV component recorded by the PMT (310 ± 6 s^{-1} rather than 3767 ± 60 s^{-1}). While this is useful, our exo-electron sensitivity is much lower than our OSL sensitivity and so it is more important to maintain exo-electron count rate than to reduce the UV background underlying the OSL signal. Using the secondary PMT provides another measure of the exo-electron signal, but it also detects a significant TL/OSL signal from the sample; this is usually much stronger than exo-electron UV signalc value.

3.3. HV switching

REES uses HV-switching to avoid contamination of the TL/OSL signal by gas fluorescence and so allows the simultaneous measurement of both TL/TSE and OSL/OSE. HV-switching is common to all anode configurations and operations of REES.

The HV modulation frequency may be varied as appropriate; for fast decaying signals, such as the OSL fast component in quartz, a high frequency is required. To test the separation of exo-electron derived signals from potential luminescence signals we use graphite; graphite contains trapping states [15] and so gives OSE but no OSL because recombination is non-luminescent, and so it can be used to demonstrate the effectiveness of the HV switching. Fig. 8a and b show that there is no detectable optical (or anode) signal when the HV is off.

The benefits of HV modulation during the measurement of TL is shown in Fig. 8c and d for a chip of synthetic quartz; the modulation allows for clear distinction between the pure TL signal from the sample during the off-period and the combined TL and UV gas fluorescence during the on-period. The corresponding effect of HV modulation during OSL measurements is shown in Fig. 8e and f.

From these data it appears that the ratio of UV fluorescence count

Table 1
Comparison of the different anode configurations and detection modes using a ^{63}Ni source operating in the GM region. The electron count rates are also give normalised to that of the linear anode.

	Ring Anode	Point Anode	PMT2 Gas Fluorescence	Linear Anode
Electron Counts [s^{-1}]	174 ± 2	54 ± 6	–	258 ± 3
UV Signal [s^{-1}]	310 ± 6	250 ± 21	57 ± 1	3767 ± 60
Normalised Efficiency	67.7 ± 1.3%	20.9 ± 2.6%	22.1 ± 0.6%	100%

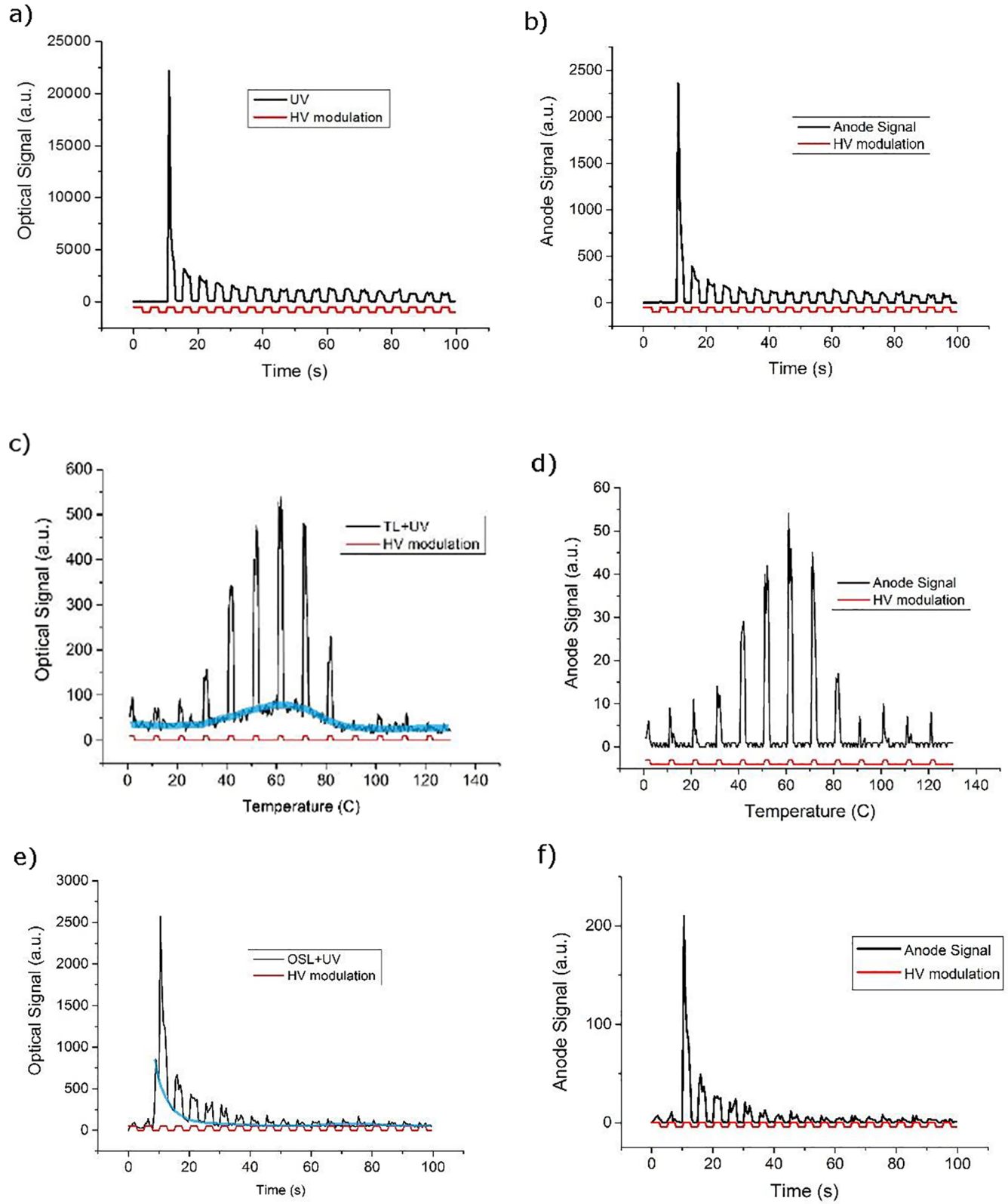

Fig. 8. Simultaneous measurement of UV (a) and OSE (b) from graphite (graphite does not produce OSL). Simultaneous TL + UV (c) and TSE (d) measurements of synthetic quartz with HV modulation, pure TL highlighted with blue. OSL + UV (e) and OSE (f) measurements on the same sample, pure OSL highlighted with blue. TL/TSE measured with a 4 channel on and 16 channels off (0.1 Hz) HV modulation. OSL/OSE measured with a 6 channel on and 5 channels off HV modulation (0.2 Hz).

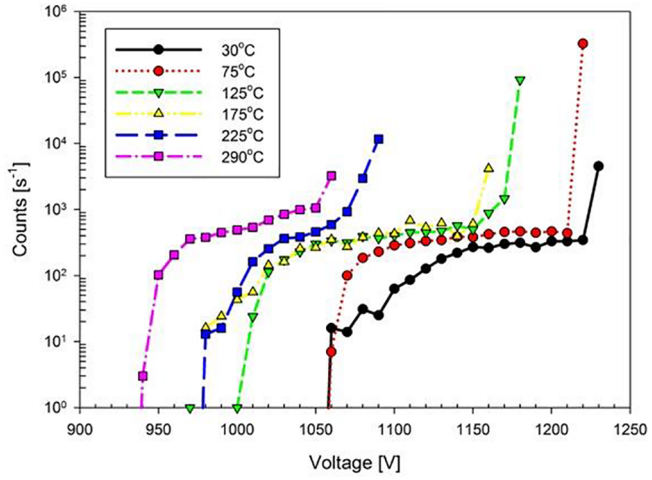

Fig. 9. The efficiency dependence on temperature for exo-electrons from quartz are very similar to those obtained for ^{63}Ni (Fig. 7) although breakdown is more clearly defined. The count rates on the plateau are also similar, although the plateaus are not as flat as in Fig. 7.

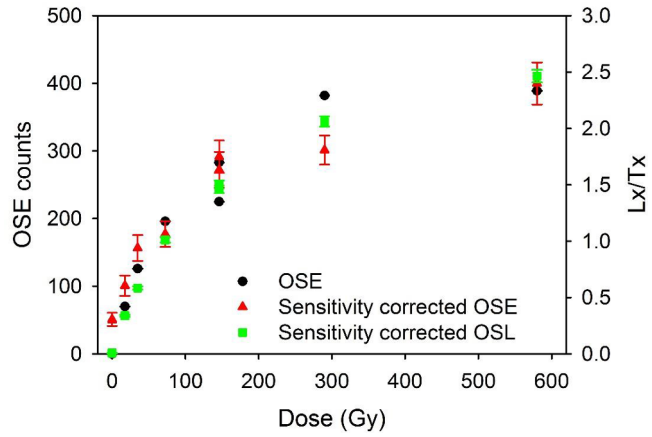

Fig. 10. Growth curves from 100 grains of calibration quartz. The curves are very similar to each other, however, sensitivity correcting the OSE signal results in a better recycling ratio (0.92 ± 0.14) than doing a simple background subtraction (0.79). Each signal has been integrated for 0.4 s and had an early background subtraction i.e. the following 0.4 s.

rate to anode signal count rate is similar for all 3 measurements, at about 10:1, suggesting considerable sensitivity advantage in using the UV signal to measure the rate of exo-electron emission. However, it must be recognised that the resulting signal is not likely to follow Poisson statistics, because each exo-electron presumably produces ~10 correlated photons.

4. Measurements on sedimentary quartz

One of the primary minerals used in luminescence dating is quartz and it is therefore important to show that REES is sufficiently sensitive to detect exo-electrons from sedimentary quartz grains.

4.1. Dependence of efficiency on temperature: exo-electrons from quartz grains on stainless steel

Efficiency curves, similar to those shown for ^{63}Ni (Fig. 7) but rather using calibration quartz [25] are shown in Fig. 9. Several hundred 180–250 μm quartz grains were placed in a clean stainless steel cup, given a beta dose of 10 Gy and then stimulated with blue LEDs at different fixed temperatures and voltages until electrical breakdown is observed (Fig. 9). As with Fig. 7, we observe that the required voltage for proportional counting decreases with increasing temperature, although without increasing the count rate in the plateau region significantly.

For a measurement temperature of 125 °C the plateau is relatively wide (~1050 to ~1140 V). This allows the operation of the detector within a range of temperatures, but with almost constant gain. For instance by setting the HV to 1150 V the detector can be operated up to 175 °C without a large change in sensitivity. However, the efficiency plateau becomes significantly narrower as the sample temperature continues to increase, making it more difficult to operate the detector without breakdown. It is also interesting that the plateau regions at the various temperatures are not as well defined as found using the ^{63}Ni beta source, and the change in absolute efficiency with temperature is somewhat larger than in Fig. 7. This may be a result of the very low residual energy with which exo-electrons are ejected into the counting gas. This would be expected to allow increased electron capture at low electron accelerations (low HV), but it is less obvious why increased gas temperature should also apparently decrease electron capture. Efficiency curves of similar form were also measured using NaCl (data not shown).

4.2. Multi-grain growth curve

The OSL/OSE response to dose of sedimentary quartz was measured using 100 grains of quartz mounted in a single-grain disc [4] following a SAR protocol [12] using a preheat of 260 °C for 10 s, and OSL/OSE measurement using the blue LEDS and the sample held at 125 °C. The OSL and OSE were sensitivity corrected using a 100 Gy test dose with a cut-heat of 220 °C. The OSL and UV signals were separated using HV modulation (1.25 Hz, 0.4 s on/0.4 s off).

Fig. 10 shows an OSE growth curve along with a sensitivity corrected OSE and OSL growth curve for the same sample. The signals were integrated for the initial 0.4 s and had an early background subtraction using the next 0.4 s. The three curves are virtually indistinguishable from one another suggesting a similar behaviour for the fast-components in both signals, as was earlier reported by [1–2].

4.3. OSL and OSE dependence on prior heating and stimulation temperature

Natural dose measurements using OSL from sedimentary quartz involve thermal pretreatment and stimulation at elevated temperature (usually 125 °C) to ensure that the OSL signal is not influenced by shallow traps (e.g. the 110 °C TL trap in quartz). Varying the preheat and/or stimulation temperature in such measurements gives insights into the origins of the stored charge giving rise to the OSL, and into the characteristics of the recombination site [14,5] p. 74; [20,21]. We chose such investigations to illustrate further the flexibility and applicability of REES in the simultaneous measurement of OSL and OSE.

Here we first examine the dependence of fast-component OSL and fast-component OSE on prior heating. A pulse anneal experiment was performed by giving a quartz aliquot a dose of 30 Gy, preheating to some temperature between 160 °C and 300 °C, and measuring the OSL and OSE with the sample held at 125 °C. A test dose of 10 Gy, preheating to 220 °C and measuring the OSL and OSE with the sample held at 125 °C was used to sensitivity correct the OSL signal (but not the OSE as this remained stable, see also [2]; the results of these experiments are shown in Fig. 11a. The sensitivity-corrected fast-component OSL remains constant between 160 °C and 250 °C; above this temperature the OSL begins to decrease due to thermal erosion of the 325 °C OSL trap [20]. However, the fast-component OSE measurements undertaken at

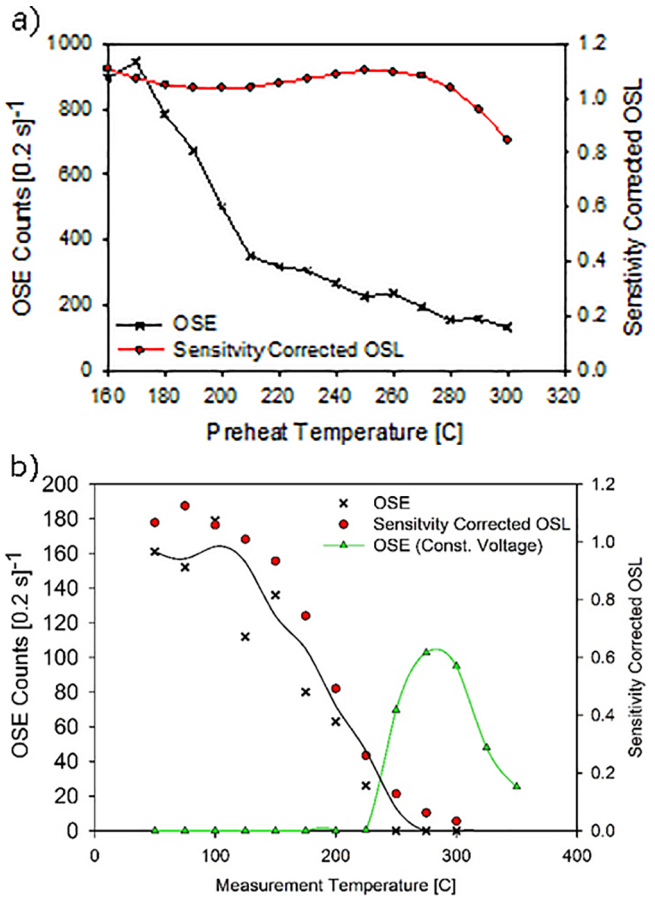

Fig. 11. Fast-component OSE and sensitivity corrected OSL as a function of preheat and measurement temperature. a) Pulse anneal measurements using a quartz aliquot measured at 125 °C. The (dimensionless) sensitivity corrected OSL (red circles) does not change significantly until 250 °C above which it starts to decline due to thermal erosion of the trap [20]. In contrast, the OSE decreases as a function of preheat temperature. b) OSL and OSE measurements of a quartz aliquot held at various temperatures during stimulation. The behaviour of the OSE signal (green triangles) when the HV is held constant and the sensitivity-corrected OSL (red circles) is consistent with that shown in Ankjærgaard et al. [2]. However, if the HV is adjusted to keep the detector on the efficiency plateau as the stimulation temperature is changed (see Fig. 9) the OSE signal (black crosses) decreases with stimulation temperature in a similar manner to the OSL. (For interpretation of the references to colour in this figure legend, the reader is referred to the web version of this article.)

the same time decrease steadily with preheat temperature, confirming the unexpected results of Ankjærgaard et al. [2].

Secondly, the effect of measurement temperature on the fast-component OSL and OSE signals was investigated by giving a quartz aliquot a dose of 30 Gy, preheating to 260 °C in order to empty shallow traps, and then performing OSL measurement at a range of temperatures from 50 °C to 300 °C. Once again, the OSL signal was sensitivity corrected using a 10 Gy test dose with a cut-heat of 220 °C and OSL measured at 125 °C.

If the HV is kept constant, the OSE and sensitivity-corrected OSL curves are consistent with those presented in Ankjærgaard et al. [2]. However, Figs. 7 and 9 show that, if the voltage is kept constant, the detector will operate with very different efficiencies as the temperature is increased. In contrast, if the detector is kept operating at a voltage within the efficiency plateau for each measurement temperature, very different results are observed (Fig. 11b, black crosses). In this case the shape of the OSE variation with temperature is very similar to that of the OSL data. Nevertheless, this result remains unexpected because the decrease in OSL is believed to be due to thermal quenching of the signal (e.g. [14,5] p. 74). If the OSE signal indeed reflects trap emptying, this suggests that, while thermal quenching presumably does occur, the fast-component trap is simultaneously emptied. Clearly the observations of Fig. 11 require further investigation but the additional use of OSE in luminescence investigations provide a pathway to understand the fundamental de-trapping mechanism which are not obvious (or unambiguous) with the of luminescence alone.

5. Conclusion

We have constructed and described a new exo-electron detection system compatible with the OSL stimulation/detection head of a Risø TL/OSL reader. This design provides a step-change improvement on the previous detector presented by Ankjærgaard et al. [1], particularly by incorporating HV-switching which allows the separation of uncontaminated luminescence signals (TL or OSL) from the UV signal generated by the corresponding exo-electrons. The detector comes with several different anode configurations; although the ring anode gives the best spatial separation of luminescence and UV fluorescence, the linear anode gives the highest counting efficiency. We have shown that it is possible to measure exo-electron signals from a laboratory pre-treated quartz with absorbed doses of a few Gy and, using HV modulation, it will be possible to resolve much lower doses by using the UV signal produced by the de-excitation of argon atoms in the gas. The improved detector has been used to repeat thermal pretreatment and elevated stimulation experiments described previously; we confirm the results of the pulse anneal experiment, but show that the previously reported discrepancy between the dependence of OSE and OSL emission on stimulation temperature was probably an experimental artefact.

Acknowledgements

M.A., N.R.J. P, and J.-P. B. receive funding from the European Research Council (ERC) under the European Union's Horizon 2020 research and innovation programme ERC-2014-StG 639904 – RELOS. The authors would like to thank C. Ankjærgaard for sharing her experience with the previous exo-electron detector, and Louise M. Helsted and Vicki Hansen for help with samples. A special thanks to Lars P. Pirtzel, Jørgen H. Jacobsen, Søren V. Dalsgaard, Finn Jørgensen and Karsten B. Nielsen for their invaluable help and knowledge in the design, construction and integration of the detector with the Risø TL/OSL reader platform and software.

References

[1] C. Ankjærgaard, A.S. Murray, P.M. Denby, L. Bøtter-Jensen, Measurement of optically and thermally stimulated electron emission from natural minerals, Radiat. Meas. 41 (2006) 780–786.
[2] C. Ankjærgaard, P.M. Denby, A.S. Murray, M. Jain, Charge movement in grains of quartz studied using exo-electron emission, Radiat. Meas. 43 (2008) 273–277.
[3] C. Ankjærgaard, A.S. Murray, P.M. Denby, M. Jain, Using optically stimulated electrons from quartz for the estimation of natural doses, Radiat. Meas. 44 (2009) 232–238.
[4] L. Bøtter-Jensen, C.E. Andersen, G.A.T. Duller, A.S. Murray, Developments in radiation, stimulation and observation facilities in luminescence measurements, Radiat. Meas. 37 (4–5) (2003) 535–541.
[5] R. Chen, S.W.S. McKeever, Theory of Thermoluminescence and Related Phenomena, World Scientific, Singapore, 1997, p. 559.
[6] J.E. Davies, Exoemission and thermoluminescence from human enamel and shark enameloid, Radiat. Prot. Dosim. 4 (3/4) (1983) 181–184.
[7] J.E. Davies, P.D. Townsend, Exoemission of Ethiopian soils and the endemicity of non-filarial elephantiasis, Radiat. Prot. Dosim. 4 (3/4) (1983) 185–188.
[8] M. Ikeya, Dating a stalactite by electron spin resonance, Nature 255 (1975) 48–50.
[9] M. Ikeya, Electron spin resonance (esr) microscopy in materials science, Annu. Rev. Mater. Sci. 21 (1991) 45–63.
[10] S.W.S. McKeever, Thermoluminescence of solids, Cambridge University Press, 1985, p. 376.

[11] B. Milsch, F. Kerbe, L. Michalowsky, Defect centres in beryllium oxide ceramic studied by electron paramagnetic resonance (EPR), Ceram. Int. 16 (1990) 311–318.
[12] A.S. Murray, A.G. Wintle, Luminescence dating of quartz using an improved single-aliquot regenerative-dose protocol, Radiat. Meas. 32 (1) (2000) 57–73.
[13] L. Oster, V. Yaskolko, J. Haddad, Classification of exoelectron emission mechanisms, Phys. Status Solidi 174 (1999) 431–439.
[14] N.A. Spooner, On the optical dating signal from quartz, Radiat. Meas. 23 (1994) 593–600.
[15] R.H. Telling, M.I. Heggie, Radiation defects in graphite, Philos. Mag. 87 (31) (2007) 4797–4846.
[16] S. Tsukamoto, A. Murray, C. Ankjærgaard, M. Jain, T. Lapp, Charge recombination processes in minerals studied using optically stimulated luminescence and time-resolved exoelectrons, J. Phys. D: Appl. Phys. 43 (2010) 325502.
[17] S. Tsukamoto, S. Toyoda, A. Tani, F. Opperman, Single aliquot regenerative dose method for ESR dating using X-ray irradiation and preheat, Radiat. Meas. 81 (2015) 9–15.
[18] S. Tsukamoto, N. Porat, C. Ankjærgaard, Dose recovery and residual dose of quartz ESR signals using modern sediments: implications for single aliquot ESR dating, Radiat. Meas. 106 (2017) 472–476.
[19] J.E. Turner, Atoms, Radiation, and Radiation Protection, second ed., John Wiley & Sons, Inc., New York, NY, USA, 1995 ISBN 0-471-59581-0.
[20] A.G. Wintle, A.S. Murray, Towards the development of a preheat procedure for OSL dating of quartz, Radiat. Meas. 29 (1998) 81–94.
[21] A.G. Wintle, A.S. Murray, Quartz OSL: effects of thermal treatment and their relevance to laboratory dating procedures, Radiat. Meas. 32 (2000) 387–400.
[22] A. Zastawny, J. Białoń, Influence of the mechanical sample treatment on the thermally stimulated exoelectron emission in aspect of the application for sample dating, Appl. Radiat. Isot.. 50 (1998) 673–676.
[23] J. Zimmerman, The radiation-induced increase of the 100°C thermoluminescence sensitivity of fired quartz, J. Phys. C: Solid St. Phys. 4 (1971) 3265–3276.
[24] K. Becker, Principles of thermally stimulated exoelectron emission (TSEE) dosimetry, IAEA Atomic Energy Rev. 8 (1970) 173–218.
[25] V. Hansen, A. Murray, J.P. Buylaert, E.Y. Yeo, K. Thomsen, A new irradiated quartz for beta source calibration, Radiat. Meas. 81 (2015) 123–127.